

Simulation of turbulent piloted methane non-premixed flame based on combination of finite-rate/eddy-dissipation model

A. Guessab*, A. Aris**, A. Bounif**

*Industrial Products and Systems Innovations Laboratory, ENPO, Oran, Algeria, E-mail: med_guessab@yahoo.fr

**Laboratoire des Carburants Gazeux et Environnement, USTOMB, Algeria, E-mail : arisaek@yahoo.fr; abdelbounif@yahoo.fr

crossref <http://dx.doi.org/10.5755/j01.mech.19.6.6000>

1. Introduction

Combustion is a complex phenomenon that is controlled by many physical processes including thermodynamics, buoyancy, chemical kinetics, radiation, mass and heat transfers and fluid mechanics. This makes conducting experiments for multi-species reacting flames extremely challenging and financially expensive. For these reasons, computer modeling of these processes is also playing a progressively important role in producing multi-scale information that is not available by using other research techniques. In many cases, numerical predictions are typically less expensive and can take less time than similar experimental programs and therefore can effectively complement experimental programs. Computational models can help in predicting flame composition, regions of high and low temperature inside the burner, and detailed composition of byproducts being produced. Detailed computational results can also help us better predict the chemical structure of flames and understand flame stabilization processes. These capabilities make Computational Fluid Dynamics (CFD) an excellent tool to complement experimental methods for understanding combustion and thus help in designing and choosing better fuel composition according to the specific needs of a burner. With the advent of more and more powerful computing resources, better algorithms, and the numerous other computational tools in the last couple of decades, CFD has evolved as a powerful tool to study and analyze combustion. However, numerous challenges are involved in making CFD a reliable and robust tool for design and engineering purposes. The numerical simulation is a useful tool because it can easily employ various conditions by simply changing the parameters. Methane is the simplest hydrocarbon fuel available; several studies have focused on methane-air flames. The oxidation of methane is quite well understood and various detailed reaction mechanisms are reported in literature [1]. They can be divided into full mechanisms, skeletal mechanisms, and reduced mechanisms. The various mechanisms differ with respect to the considered species and reactions. However, considering the uncertainties and simplifications included in a turbulent flame calculation, the various mechanisms agree reasonably well [2]. In literature, several mechanisms of methane combustion exist. We can cite: for detailed mechanisms: Westbrook [3], Glarborg et al. [4], Miller and Bowman [5], and recently, Konnov et al. [6], Huges et al. [7], LCSR [8], Leeds v.1.5 [9], San Diego [10] and the standard GRI-Mech v.3.0 [11], GRI-Mech v.1.2 [12] for reduced mechanisms: Westbrook and Dryer [13], and Jones and Lindstedt [14] (more

than 2 global reaction). For skeletal mechanisms: Kazakov and Frenklach [15], Yungster and Rabinowitz [16], Petersen and Hanson [17], Hyer *et al.* [18] and Li and Williams [19].

The objective of this study was to investigate how simplified kinetics mechanisms performed in comparison to the fast chemistry assumption when simulating a piloted CH₄ nonpremixed flame with RANS and hybrid Finite-Rate/Eddy Dissipation model. A one-step mechanism by Westbrook and Dryer [13] and the four-step mechanism suggested by Jones and Lindstedt [14] were chosen for comparison. Finally, Fluent is used for this study with some modifications of the usually adopted models for the representations of the turbulence-kinetics interaction are introduced (UDF for Hybrid Finite-Rate/Eddy Dissipation model). The results were compared with experimental data [20].

2. Numerical modeling

2.1. Mathematical formulation

The numerical model solves the independent time equations for conservation of mass, momentum, energy and individual species:

$$\nabla \cdot (\rho \vec{v}) = 0; \quad (1)$$

$$\nabla \cdot (\rho \vec{v} \vec{v}) = -\nabla P + \nabla \cdot (\tau) + \rho \vec{g}; \quad (2)$$

$$\begin{aligned} \frac{\partial (\rho U_i E)}{\partial x_i} = \\ = \frac{\partial}{\partial x_i} \left[\alpha_{eff} \frac{\partial T}{\partial x_i} - \sum h_j J_j + U_i (\tau_{ij})_{eff} \right] + S_h, \end{aligned} \quad (3)$$

where:

$$E = h - \frac{P}{h} + \frac{U_i^2}{2}; \quad (4)$$

$$h = \sum_i m_i h_i; \quad (5)$$

$$h_i = \int_{T_{ref}}^T C_{p_i} \partial T \quad (T_{ref} = 298.15 \text{ K}); \quad (6)$$

$$S_h = -\sum_j \left(\frac{h_j^0}{M_j} + \int_{T_{ref}}^T C_{p_i} dT \right) R_i; \quad (7)$$

$$J_i = -\left(\rho D_{i,m} + \frac{\mu_t}{Sc_t}\right) \frac{\partial Y_i}{\partial x_i}; \quad (8)$$

$$\left(\tau_{ij}\right)_{eff} = \mu_{eff} \left(\frac{U_j}{x_i} + \frac{U_i}{x_j}\right) - \frac{2}{3} \mu_{eff} \frac{U_i}{x_i} \delta_{ij}; \quad (9)$$

$$\alpha_{eff} = \alpha + \alpha_t. \quad (10)$$

2.2. Species transport and reaction

$$\frac{\partial(\rho V_j Y_i)}{\partial x_i} = -\frac{\partial^2}{\partial x_i^2} \left[\left(\rho D_{i,m} + \frac{\mu_t}{Sc_t}\right) Y_i \right] + R_i + S_i, \quad (11)$$

where R_i is the chemical production rate; Sc_t is number turbulent of Schmidt $\mu_t / (\rho D_t)$; S_i is includes all other sources.

2.3. Heat radiation

The radiative heat flux q_r is expressed as follows:

$$q_r = -4\sigma \sum (P_i a_{p,i}) (T^4 - T_{abm}^4), \quad (12)$$

where σ is the Stefan–Boltzmann constant and p_i the partial pressure of species i . $a_{p,i}$ is the Plank mean absorption coefficients for radiating species i [22] and P the static pressure, g term of gravity, Y_i is the mass fraction, $D_{i,m}$ the thermal diffusivity, T the temperature, ρ the density, h the specific enthalpy, m_i the mass flux of fuel. Radiation/absorption in gas is neglected.

2.4. Turbulence modeling

The standard $k-\varepsilon$ model (include a correction for round jets performed by using the Pope formulation) turbulence closure model is adopted. In the $k-\varepsilon$ model the Reynolds stress is closed using mean velocity gradients employing Boussinesq hypothesis [22]. In the case of a jet flame, a correction is necessary to accurately predict the spreading rate of the jet. This is performed by using the Pope correction, P_{pc} , as an additional term in the equation of turbulence dissipation rate (ε) [22]:

$$P_{PC} = \bar{\rho} C_{\varepsilon 3} \frac{\varepsilon^2}{k} S_\varepsilon. \quad (13)$$

The term S_ε can be written as (Pope, 1978):

$$S_\varepsilon = \omega_{ij} \omega_{jk} S_{ij}, \quad (14)$$

where

$$S_{ij} = \frac{1}{2} \frac{k}{\varepsilon} \left(\frac{\partial u_i}{\partial x_j} + \frac{\partial u_j}{\partial x_i} \right). \quad (15)$$

$$\omega_{ij} = \frac{1}{2} \frac{k}{\varepsilon} \left(\frac{\partial u_i}{\partial x_j} - \frac{\partial u_j}{\partial x_i} \right), \quad (16)$$

where $C_{\varepsilon 3} = 0.79$, the standard model constants have been chosen. As an option in the formulation of the $k-\varepsilon$ model, enhanced wall functions were selected in accordance with the grid design. This option ensured that appropriate modeling occurred to resolve the viscous sub-layer.

3. Problem description

The flame simulations were performed and compared with experimental data from literature [20]. The flame is a turbulent non-premixed piloted methane flame. A co-flowing air was placed around the flame to avoid the influence of air flow in radial direction. The boundary conditions of the measurements are shown in Table 1.

Table 1
Experimental and simulation condistions [20]

Jet diameter, D_{jet} , mm	7.2
Pilot inner diameter, $D_{p,i}$, mm	7.7
Pilot diameter, $D_{p,o}$, mm	18.2
Burner outer wall diameter, $D_{B,o}$, mm	18.9
Jet Reynolds number, Re	22400
U_{coflow} , m/s, T_{coflow} , K	0.9, 291
Jet composition CH_4/air (volume fraction)	25/75
U_{jet} , m/s, T_{jet} , K	49.6, 294
U_p , m/s, T_p , K	11.4, 1880

The geometrical configuration of the burner for predicted CH_4/air turbulent combustion is that reported in (Fig. 1). The geometry for this test is a cylindrical combustor with coaxial injectors, where the natural gas is injected by the primary tube and the air piloted flow through the secondary annulus. In the fuel stream, the uniforme inlet gas velocity is 49.6 m/s with a temperature of 294 K. The Co-flowing air parallel to the flame was about 0.9 m/s with a preheated temperature of 291 K. The Reynolds number of the jet exit is 22400 with a low probability of localized flame extinction. The pilot flame burns a mixture of gases having the same composition and enthalpy as a CH_4/air mixture at 0.27 mixture fraction. The experiment was performed at pressure atmospheric.

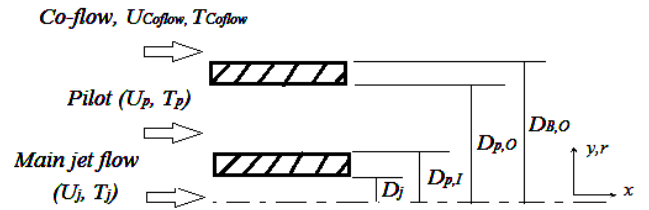


Fig. 1 Geometry of the coaxial combustor [20]

In the present computation, the reaction rate are computed by combination of Finite-Rate and Eddy-dissipation model for turbulent flow, both the Arrhenius rate and mixing rate are computed and smaller of the two is used. The specific heat values for the species are defined as piecewise-polynomial function of temperature.

3.1. The laminar finite rate model (source of species)

The laminar finite-rate model computes the chemical source terms using Arrhenius expressions, and ignores the effects of turbulent fluctuations.

The model is exact for laminar flames, but is gen-

erally inaccurate for turbulent flames due to highly non-linear Arrhenius chemical kinetics. The net source of chemical species i due to reaction am computed the sum of the Arrhenius reaction sources over the N_R reactions that the species may participate in:

$$\hat{R}_i = M_{w,i} \sum_{k=1}^{N_R} \hat{R}_{i,k}, \quad (17)$$

where $M_{w,i}$ is the molecular mass of species i and $\hat{R}_{i,k}$ is the molar rate of creation/destruction of species i in reaction k . Reaction may occur in the continuous phase between continuous phase species only, or at resulting in the surface deposition or evolution of a continuous-phase species. The reaction rate, $\hat{R}_{i,k}$ is controlled either by an Arrhenius kinetic rate expression or by mixing of the turbulent eddies containing fluctuating species concentrations.

3.2. The arrhenius rate (chemical kinetics)

Chemical kinetic governs the behavior of reacting chemical species. As explained earlier, a combustion reaction proceeds over many reaction steps, characterized by the production and consumption of intermediate reactants. Several conditions determining the rate of reaction are the concentration of reactants and the temperature. The concentration of the reactants affects the probability of reactant collision, while the temperature determines the probability of the reaction occurring given a collision. In general, a chemical reaction can be written in the form as follows:



where N is number of chemical species in the system; $v'_{i,k}$ is Stoichiometric coef. for reactant i in reaction k ; $v''_{i,k}$ is Stoichiometric coef. for product i in reaction k ; A_i is chemical symbol denoting species i ; $k_{f,k}$ is forward rate constant for reaction k ; $k_{b,k}$ is backward rate constant for reaction k .

Eq. (18) is valid for both reversible and non-reversible reactions. For non-reversible reactions, the backward rate constant $k_{b,k}$ is simply omitted. The summations in Eq. (18) are for all chemical species in the system, but only species involved as reactants or products will have non-zero stoichiometric coefficients. Hence, species that are not involved will drop of the equation except for third-body reaction species.

3.3. Reaction rate

The molar rate of creation/destruction of species i' in reaction k , $\hat{R}_{i',k}$, in Eq. (17) $\hat{R}_{i',k}$ is given by:

$$\hat{R}_{i',k} = \Gamma (v''_{i',k} - v'_{i',k}) \times \left(k_{f,k} \prod_{j=1}^N [C_j]^{\eta'_{j,k}} - k_{b,k} \prod_{j=1}^N [C_j]^{\eta''_{j,k}} \right), \quad (19)$$

where C_j is molar concentration of each reactant or product species j , Kmol m^{-3} ; $\eta'_{j,k}$ is rate exponent for reactant j' in reaction k ; $\eta''_{j,k}$ is rate exponent for product j' in reaction k ; Γ is represents the net effect of third bodies on the reaction rate. This term is given by:

$$\Gamma = \sum_{j'}^N \gamma_{j',k} C_j, \quad (20)$$

where $\gamma_{j',k}$ is the third-body efficiency of the j' th species in the k -th reaction. The forward rate constant for reaction k , $k_{f,k}$, is computed using the Arrhenius expression

$$k_{f,k} = A_k T^{\beta_k} \exp(-E_k / (RT)), \quad (21)$$

where A_k is pre-exponential factor (consistent units); β_k is temperature exponent (dimensionless); E_k is activation energy for the reaction, J Kgmol^{-1} ; R is universal gas constant (8313), $\text{J Kmol}^{-1}\text{K}^{-1}$.

The values of $v'_{i,k}$, $v''_{i,k}$, $\eta'_{i,k}$, $\eta''_{i,k}$, β_k , A_k , E_k and $\gamma_{j',k}$ can be provided the problem definition. If the reaction is reversible, the backward rate constant for reaction k , $k_{b,k}$, is computed from the forward rate constant using the following relation:

$$k_{b,k} = \frac{k_{f,k}}{K_k}, \quad (22)$$

where K_k is the equilibrium constant for the k -th reaction. Computed from:

$$K_k = \exp\left(\frac{\Delta S_k^0}{R} - \frac{\Delta H_k^0}{RT}\right) \left(\frac{P_{atm}}{RT}\right)^{\sum_{k=1}^{NR} (v''_{i,k} - v'_{i,k})}, \quad (23)$$

where P_{atm} denotes atmospheric pressure (101325 Pa). The term within the exponential represents the change in Gibbs free energy, and its components are computed as follows:

$$\frac{\Delta S_k^0}{R} = \sum_{i'=1}^N (v''_{i',k} - v'_{i',k}) \frac{S_{i'}^0}{R}; \quad (24)$$

$$\frac{\Delta H_k^0}{RT} = \sum_{i'=1}^N (v''_{i',k} - v'_{i',k}) \frac{h_{i'}^0}{RT}, \quad (25)$$

where $S_{i'}^0$ and $h_{i'}^0$ are, respectively, the standard-state entropy and standard-state enthalpy including heat of formation. These values are specified in Fluent.

3.4. The eddy dissipation model (EDM)

Fluent provides a turbulence-chemistry interaction model, based on the work of Magnussen and Hjertager [21], called the eddy-dissipation model. The rate of production of species i due to reaction, R_i , is given by the smaller of the two expressions below:

$$R_i = \min \left\{ \begin{array}{l} \nu'_{i,k} M_i A \rho \frac{\varepsilon}{k} \left(\frac{Y_R}{\nu'_{R,k} M_R} \right), \\ \nu'_{i,k} M_i A B \rho \frac{\varepsilon}{k} \left(\frac{\sum_P Y_P}{\sum_j^N \nu''_{j,k} M_j} \right) \end{array} \right\}, \quad (26)$$

where A is Magnussen constant for reactants (default 4.0); B is Magnussen constant for products (default 0.5); M is molecular mass of species; $(R), (P)$ is reactants, products; ν'_i, ν''_j are stoichiometric coefficient for reactant i and product j in reaction.

3.5. Combustion model

The turbulent non-premixed combustion process is simulated using the hybrid Finite-Rate/Eddy-Dissipation model [22]. The fuel is assumed to burn by a 1-step and 4-step chemical reaction. For the 1-step reaction, the global chemical kinetics scheme of Westbrook and Dryer (Table 2) was used to describe the combustion process in terms of 5 species ($\text{CH}_4, \text{CO}_2, \text{H}_2\text{O}, \text{O}_2$ and N_2 as inert). For the 4-step reaction, the reduced chemical kinetics scheme of Jones and Lindstedt (Table 3) was used to describe the combustion process in terms of 7 species ($\text{CH}_4, \text{CO}_2, \text{H}_2\text{O}, \text{O}_2, \text{CO}, \text{H}_2$ and N_2 as inert).

3.6. Finite-rate/eddy-dissipation model (FR-EDM)

The Eddy-Dissipation Model assumes that reactions are fast and that the system is purely mixing limited and when that is not the case, it can be combined with finite-rate chemistry. In that case, the kinetic rate is calculated in addition to the reaction rate predicted by the eddy-dissipation model. The slowest reaction rate is then used: if turbulence is low, mixing is slow and this will limit the reaction rate. If turbulence is high, but the kinetic rate is low, this will limit the reaction rate. This model can be used for a variety of systems, but with the following caveats: the model constants A and B need to be empirically adjusted for each reaction in each system. The default values of 4.0 and 0.5 respectively were determined for one and two-step combustion processes. The model (FR-EDM) always requires some product to be present for reactions to proceed. If this is not desirable, initial mass fractions of product of $1\text{E-}10$ can be patched and a model constant $B = 1\text{E}10$ used.

4. Simulation detail

The governing equations are solved using the

ANSYS-FLUENT CFD package modified with User-Defined Functions (UDF) in order to integrate the reaction rate formula proposed by Jones and Lindstedt [14]. In computational fluid dynamics, the differential equations govern the problem are discretized into finite volume and then solved using algebraic approximations of differential equations. These numerical approximations of the solution are then iterated until adequate flow convergence is reached. The chemical kinetics information is then coupled into fluid dynamics equations to allow both phenomena to be incorporate into a single problem. SIPMLE algorithm [22] was chosen for the coupling between the velocity and the pressure. For all simulations presented in this paper, a First Order Upwind scheme was used for all the conservation equations ($U, V, E, Y_i, k, \varepsilon$ and $P1$). The Standard scheme [22] was used for interpolation methods for pressure. This means that the solution approximation in each finite volume was assumed to be linear. This saved on computational expense. In order to properly justify using a first order scheme, it was necessary to show that the grid used in this work had adequate resolution to accurately capture the physics occurring within the domain. In other words, the results needed to be independent of the grid resolution. This was verified by running simulations with higher resolution grids. In a reacting flow such as that studied in this work, there are significant time scale differences between the general flow characteristics and the chemical reactions. In order to handle the numerical difficulties that arise from this, the STIFF Chemistry Solver was enabled in Fluent. For more information about this technique refer to [22]. The criterion of convergence is the summation of residual mass sources less than 10^{-3} for the other terms of the transport equations and is 10^{-6} for energy equation. The criterion of convergence is the summation of residual mass sources less than 10^{-3} for the other terms of the transport equations and is 10^{-6} for energy equation. The options used in this work are presented in Table 4. The computational space seen in Fig. 1 given a finite volume mesh is divided by a staggered non-uniform quadrilateral cell (Fig. 2). A total number of 640 (32×20) quadrilateral cells were generated using non-uniform grid spacing to provide an adequate resolution near the jet axis and close to the burner where gradients were large. The grid spacing increased in the radial and axial directions since gradients were small in the far-field. The combustion will be modeled using 1-step global mechanism and reduced 4-step reaction mechanism and the radiative heat transfer of the piloted flames is calculated with the $P1$ model [22]. The interaction between turbulence and chemistry is often handled through the Finite-Rate/Eddy-Dissipation Model.

Table 2

Westbrook and dryer global chemical kinetics mechanism for CH_4/air combustion and reaction rate coefficients [13]

No.	Reaction	A_k	β_k	E_k	Reaction orders
WD1	$\text{CH}_4 + 2\text{O}_2 \rightarrow \text{CO}_2 + 2\text{H}_2\text{O}$	1.0e+12	0	1.0e+08	$[\text{CH}_4]^{0.5} [\text{O}_2]^{1.25}$

Jones and Lindstedt reduced multi-step chemical kinetics mechanism for CH₄/air combustion and reaction rate coefficients [14]

No.	Reaction	A_k , cgs units	β_k	E_k , cal/mol	Reaction orders
JL1 JL2	$\text{CH}_4 + 0.5\text{O}_2 \rightarrow \text{CO} + 2\text{H}_2$ $\text{CH}_4 + \text{H}_2\text{O} \rightarrow \text{CO} + 3\text{H}_2$	7.82e+13	0	30.0e+03	$[\text{CH}_4]^{10.5} [\text{O}_2]^{1.25}$
JL3	$\text{H}_2 + 0.5\text{O}_2 \rightarrow \text{H}_2\text{O}$	3.0e+11	0	30.0e+03	$[\text{CH}_4][\text{H}_2\text{O}]$
JL4	$\text{CO} + \text{H}_2\text{O} \rightarrow \text{CO}_2 + \text{H}_2$	1.21e+18	-1	40.0e+03	$[\text{H}_2]^{0.25} [\text{O}_2]^{1.5}$
		2.75e+12	0	20.0e+03	$[\text{CO}][\text{H}_2\text{O}]$

Table 4
Under-relaxation factors and discretization model step (F.O.U = First-Order-Upwind)

Pressure	0.3	Solver Type	Pressure based
Density	0.5	Viscous model	$k-\varepsilon$
Body forces	1	Gravitational effect	On
Momentum	0.7	2d-space	axisymmetric
Turbulent viscosity	1	Pressure-velocity coupling	Simple
Y_i	0.9	Pressure model	Standard
Energy	0.4	Energy	F.O.U.
Turbulent kinetic energy ' k '	0.8	Turbulent kinetic energy ' k '	F.O.U.
Turbulent dissipation rate ' ε '	0.8	Turbulent dissipation rate ' ε '	F.O.U.
Radiation model ' $P1$ '	0.8	Radiation model ' $P1$ '	F.O.U.

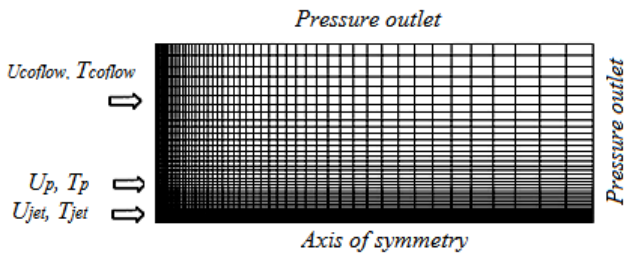


Fig. 2 Computational mesh and the boundary conditions

5. Results

We begin by comparing the computational cost of the two kinetic models in terms of the average CPU (execution) time per time step (s). The relative elapsed CPU times are compared in Table 5. In the 4-step mechanism, more reaction equations are computed, then more CPU time is spent and more difficult it is to convergence. That in general the computational cost increases with the number of reaction-step and species and more difficult it is to convergence.

Table 5
Average execution time per time step

Mechanism	Species	React.	CPU (s)	Iterat.
1-step 'WD'	05	01	0.00398	569
4-step 'JL'	07	04	0.058897	2356

5.1. Temperature field

Fig. 3 show the contour plot of the temperature for Westbrook and Dryer 'WD' (Fig. 3, a) and Jones and Lindstedt 'JL' mechanism (Fig. 3, b), respectively. It is

observed that the temperature is over predicted with the 'WD' mechanism and the temperature profile is quite flat for a wide region. In case of the 'JL' mechanism the temperature are also over predicted. It is noticed that the smallest flame is predicted by the 1-step model 'WD', whereas the largest flame is predicted by the 4-step model 'JL'. The axial distribution of the mean temperature is represented in (Fig. 4). One-step 'WD' and four-step 'JL' model all predict the peak of temperature distribution and the predicted peaks are all near the position of the experimental one: $x / D_{jet} = 47$.

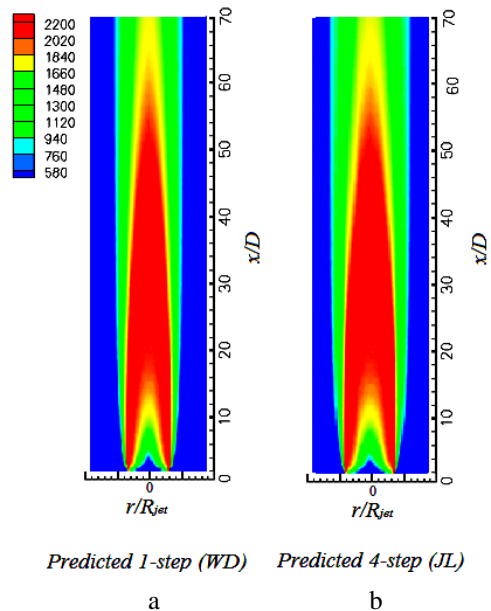


Fig. 3 Instantaneous temperature in Kelvin contour plot with the 'WD' mechanism a) and 'JL' mechanism b)

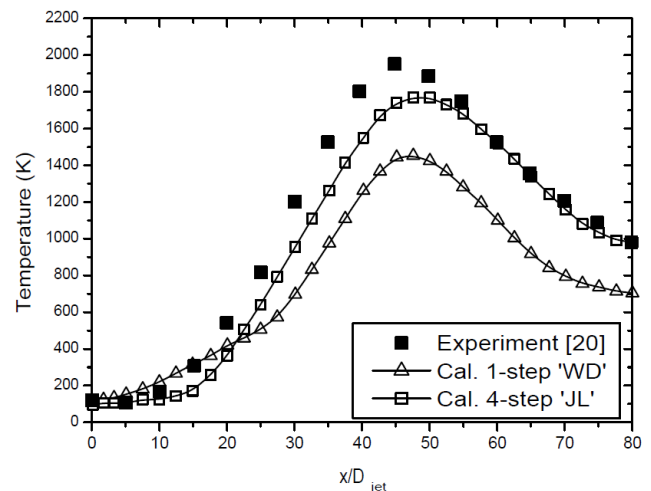


Fig. 4 Comparison of the axial temperature profiles with experimental data

The radial distribution of the mean temperature is represented in (Figs. 5-7) using two mechanisms have the same right trend; however, quantitatively the 4-step scheme (J-L mechanism) gives the best agreement with experimental data and along the radial coordinate, the temperature profiles move from the highest values, characteristic of the hot core of the flame to the decrease and then finally to the asymptotic value which refers to the recirculating exhausted gas.

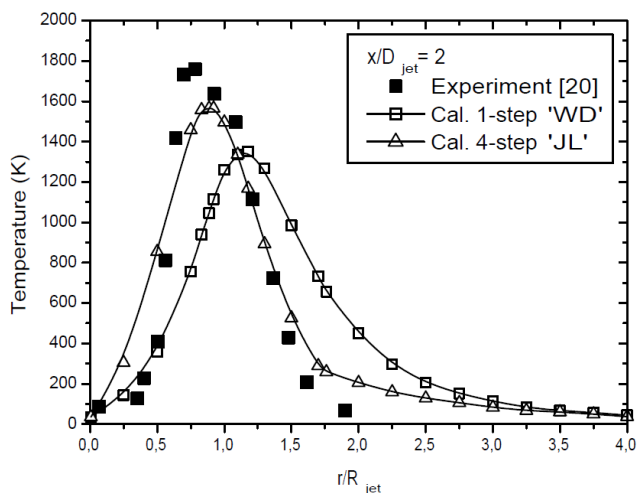


Fig. 5 Temperature profile at $x/D_{jet} = 2$

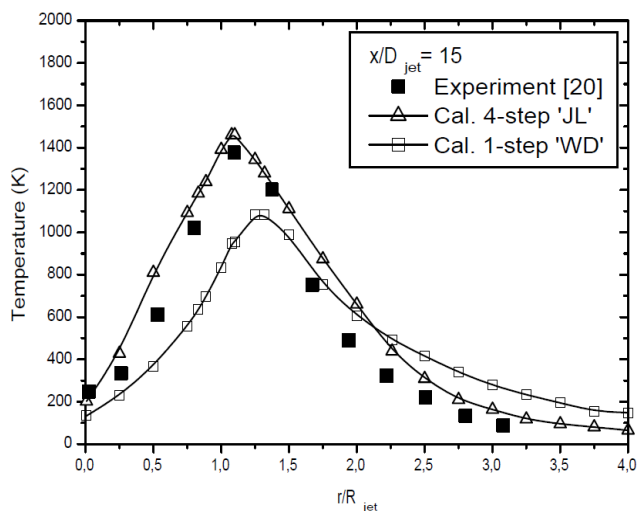


Fig. 6 Temperature profile at $x/D_{jet} = 15$

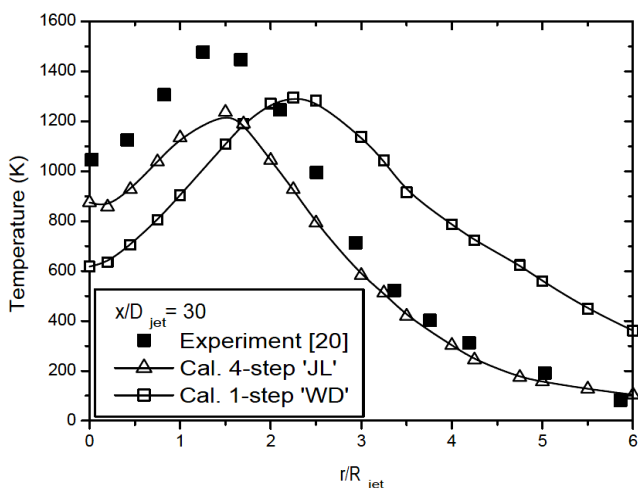


Fig. 7 Temperature profile at $x/D_{jet} = 30$

5.2. Mass fraction of H₂O

Fig. 8 show the centerline profiles of the concentration of H₂O. It is observed that with 'JL' and 'WD' mechanism at high equivalence region ($x/D_{jet} \leq 45$), the H₂O mass fraction are predicted reasonably well, and for low equivalence regime ($x/D_{jet} \geq 45$) the H₂O mass fraction are over predicted compared to the experiments.

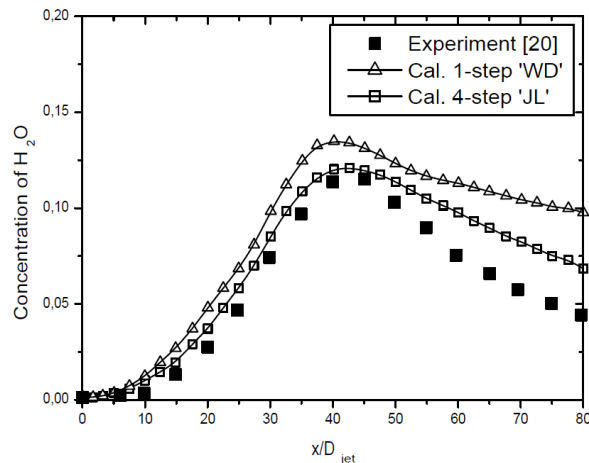


Fig. 8 Center line profile the concentration of H₂O

5.3. CH₄ and O₂ concentrations profiles

Figs. 9-13 shows CH₄ and O₂ concentration profiles. The axial distribution of the concentration of CH₄ is represented in (Fig. 8).

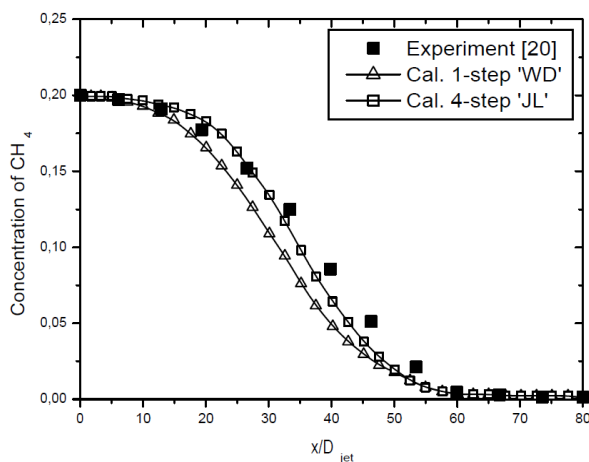


Fig. 9 Axial concentration of CH₄

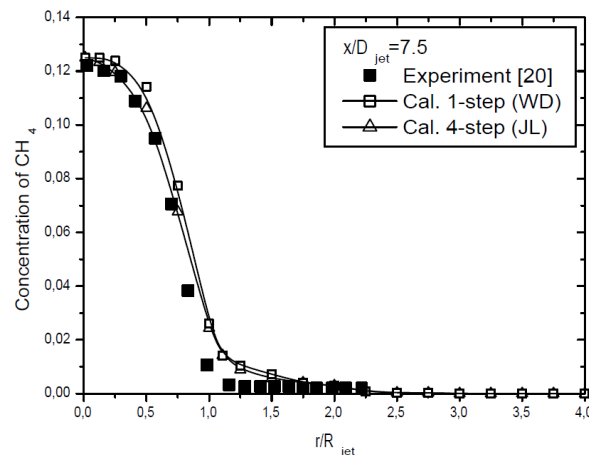


Fig. 10 CH₄ concentration profile at $x/D_{jet} = 7.5$

The concentration of CH_4 is good estimated with 1-step and 4-step reaction scheme in the inner recirculation zone $x/D_{jet} = 7.5$ (Fig. 9), where fuel is mixed into the flow. Once again, the 4-step global mechanism gives the best results to predicted CH_4 concentration (Figs. 10 and 11). Using the 1-step is much larger than measured, since the fuel is much less consumed under the much lower reaction rate provided by the 1-step mechanism model. Similar results are obtained for oxygen concentration profiles (Figs. 11 and 12).

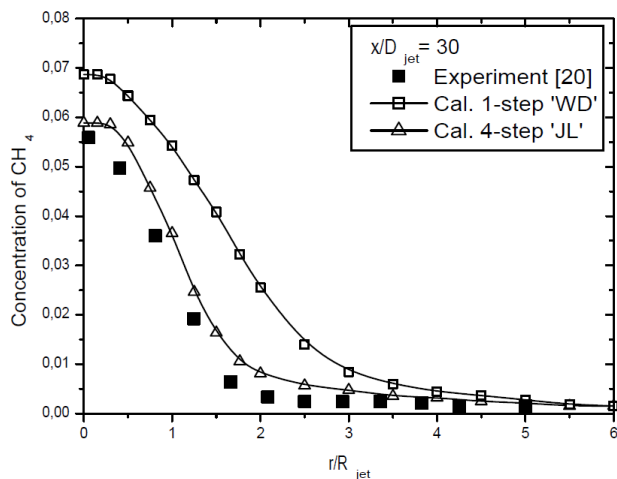


Fig. 11 CH_4 concentration profile at $x/D_{jet} = 30$

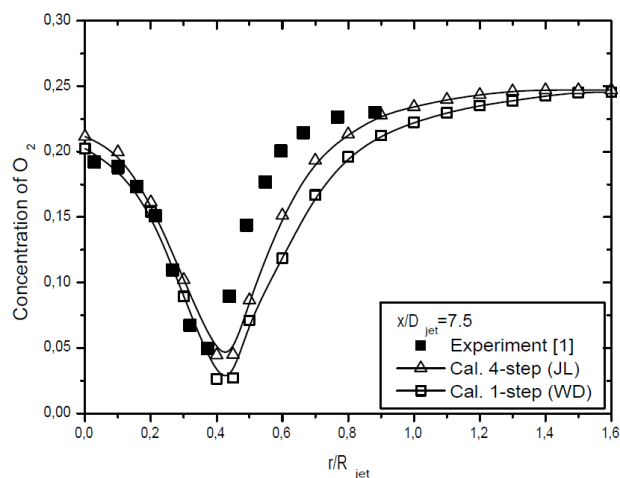


Fig. 12 O_2 concentration profile at $x/D_{jet} = 7.5$

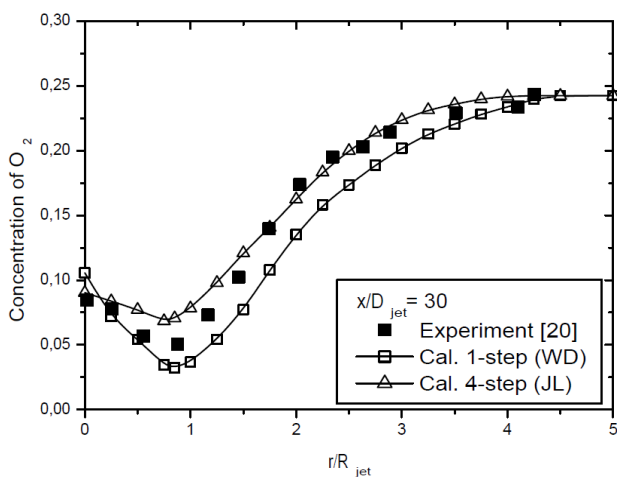


Fig. 13 O_2 concentration profile at $x/D_{jet} = 30$

6. Conclusion

In the present work the applicability of two different kinetic mechanisms: global mechanism of Westbrook and Dryer 'WD' and reduced mechanism of Jones and Lindstedt, 'JL' on the predictions of a piloted non-premixed turbulent flame to account for an accurate prediction of the flow and temperature field of a jet flame was investigated. The 7 species reduced mechanism was successfully implemented and tested with the global mechanism into the CFD solver Fluent. The precompiled mechanism was linked to the solver by the means of User Defined Function (UDF). This implemented was tested with the Barlow Piloted CH_4/air flame. In general, in the 4-step mechanism, the presence of CO and H_2 lowers the total heat release and the adiabatic flame temperature is below the values predicted by the 1-step global mechanism and the smallest flame is predicted by the global reaction, whereas the largest flame is predicted by the 4-step mechanism.

References

1. Magel, H.C.; Schnell, H.; Hein, K.R.C. 1997. Simulation of detailed chemistry in a turbulent combustion flow, Proceedings, 26th Symposium (International) on Combustion, Neapel, Italy, (1996), The Combustion Institute, Pittsburgh, Penn., USA, 67-74.
2. Davidenko, D.M.; Gökalp, I.; Dufour, E.; Magre, P. 2005. Numerical simulation of supersonic combustion with $\text{CH}_4\text{-H}_2$ fuel, European Conference for Aerospace Sciences (EUCASS), Moscow, Russia, 4-7 July.
3. Westbrook, C.K. 1985. Applying Chemical Kinetics to Natural Gas Combustion Problems, Report No. PB-86-168770/XAB, Lawrence Livermore National Laboratory, Livermore, Cal., USA.
4. Glarborg, P.; Miller, J.A.; Kee, R.J. 1986. Kinetic modeling and sensitivity analysis of nitrogen oxide formation in well stirred reactors, Combustion and Flame 65(2): 177-202.
[http://dx.doi.org/10.1016/0010-2180\(86\)90018-0](http://dx.doi.org/10.1016/0010-2180(86)90018-0).
5. Miller, J.A.; Bowman, C.T. 1989. Mechanism and modeling of nitrogen chemistry in combustion, Progress in Energy and Combustion Sciences 15(4): 287-338.
[http://dx.doi.org/10.1016/0360-1285\(89\)90017-8](http://dx.doi.org/10.1016/0360-1285(89)90017-8).
6. Konnov, A.A.; Dyakov, I.V.; DE Bruck, J. 2001. Measurement of adiabatic burning velocity and probe sampling in methane-oxygen-carbon dioxide mixtures, Proceedings of the 17th Intern. Symp. On Comb. Prec., Poznan, Poland, 171-177.
7. Huges, K.J.; et. al. 2001. Development and testing of a comprehensive chemical mechanism for the oxidation of methane, International Journal of Chemical Kinetics 33(9): 515-538.
8. Dagaut, P. 2002. On the kinetics of hydrocarbon oxidation from natural gas to kerosene and diesel fuel, Phys. Chem. Chem. Phys. 4: 2079-2094.
<http://dx.doi.org/10.1039/b110787a>.
9. The Leeds methane oxidation mechanism, <http://garfield.chem.elte.hu/Combustion/methane.htm>.
10. San Diego Mechanism 2003.
<http://web.eng.ucsd.edu/mae/groups/combustion/mechanism.html>.

11. GRI-Mech v.3.0,
http://www.me.berkeley.edu/gri_mech/.
12. **Frenklach, M.; Wang, H.; Yu, C.-L.; Goldenberg, M.; Bowman, C.T.; Hanson, R.K.; Davidson, D.F.; Chang, E.J.; Smith, G.P.; Golden, D.M.; Gardiner, W.C.; Lissianski, V.** http://diesel.me.berkeley.edu/~gri_mech/new21/version12/text12.html.
13. **Westbrook, C.K.; Dryer, F.L.** 1981. Simplified reaction mechanisms for the oxidation of hydrocarbon fuels in flames, *Combustion Sciences and Technologies* 27(1-2): 31-43.
<http://dx.doi.org/10.1080/00102208108946970>.
14. **Jones, W.P.; Lindstedt, R.P.** 1988. Global reaction schemes for hydrocarbon combustion, *Combustion and Flame* 73(3): 233-249.
[http://dx.doi.org/10.1016/0010-2180\(88\)90021-1](http://dx.doi.org/10.1016/0010-2180(88)90021-1).
15. **Kazakov, A.; Frenklach, M.** Reduced Reaction Sets based on GRI-Mech 1.2, <http://www.me.berkeley.edu/drm/>
16. **Yungster, S.; Rabinowitz, M.J.** 1994. Computation of shock-induced combustion using a detailed methane-air mechanism, *Journal of Propulsion and Power* 10(5): 609-617.
<http://dx.doi.org/10.2514/3.23770>.
17. **Petersen, E.L.; Hanson, R.K.** 1999. Reduced kinetics mechanisms for ram accelerator combustion, *Journal of Propulsion and Power* 15(4): 591-600.
<http://dx.doi.org/10.2514/2.5468>.
18. **Hyer, P.; Stocker, D.; Clar, I.O.** 1991. Gravitational Effects on Laminar Diffusion Flames, *Creare. X Users' Group Meeting Proceedings*, 345-372.
19. **Li, S.C.; Williams, F.A.** 2002. Reaction mechanisms for methane ignition, *Journal of Engineering for Gas Turbines and Power* 124: 471-480.
<http://dx.doi.org/10.1115/1.1377871>.
20. **Barlow, R.; Chen, J-Y.; Bilger, R.; et al.** Sandia Piloted CH_4 /Air Jet Flame: Preliminary Data release, 3rd International Workshop on Measurement and Computation of Turbulent Nonpremixed Flames.
<http://www.ca.sandia.gov/Workshop/Workshop.html>.
21. **Magnussen, B.; Hjertager, B.H.** 1976. 16th symposium (int.) on combustion, The Combustion Institute, Pittsburgh, 719-729.
22. **FLUENT.** 2009. "Theory Guide: Release 12.0." Last-modified January 23, 2009.

A. Guessab, A. Aris, A. Bounif

TURBULENTINĖS VALDOMOS NESUMAIŠYTOS METANO - ORO LIEPSNOS, SUFORMUOTOS NAUDOJANT BAIGTINIO GREIČIO SŪKURINĖS SKLAIDOS MODELĮ, TYRIMAS

Re z i u m ė

Naudojant valdomą simetrinę turbulentinę nesumaišytą liepsną buvo testuojami ir lyginami du metano degimo cheminiai kinetiniai mechanizmai: 1-ojo žingsnio (pagal Westbrooką ir Dryerį) ir 4-ojo žingsnio (pagal Jonesą ir Lindstedtą) temperatūros ir molekulių rūšies pasiskirstymas. Skaičiavimo rezultatai palyginti su eksperimentiniais. 4-ojo žingsnio metano degimo mechanizmas buvo sėkmingai įdiegtas į skaitmeninę skysčio dinamikos programą Fluent. Skaitmeninis sprendinys gerai dera su 4-ojo žingsnio degimo mechanizmo eksperimentiniais rezultatais.

A. Guessab, A. Aris, A. Bounif

SIMULATION OF TURBULENT PILOTED METHANE NONPREMIXED FLAME BASED ON COMBINATION OF FINITE-RATE/EDDY DISSIPATION MODEL

S u m m a r y

Two chemical kinetic mechanisms of methane combustion were tested and compared using a piloted axisymmetric turbulent non-premixed flame: 1-step and 4-step mechanism, to predict the temperature and species distributions. The numerical results are presented and compared with the experimental data. A 4-step methane mechanism was successfully implanted into CFD solver Fluent. The numerical solution is in very good agreement with previous numeral of 4-step mechanism and the experimental data.

Keywords: RANS, Mechanism, FR-EDM, Simulation.

Received November 23, 2012

Accepted November 11, 2013